scientific reports

Check for updates

OPEN

Rab11-dependent recycling of calcium channels is mediated by auxiliary subunit $\alpha_2\delta$-1 but not $\alpha_2\delta$-3

James O. Meyer & Annette C. Dolphin ✉

N-type voltage-gated calcium channels ($Ca_V2.2$) are predominantly expressed at presynaptic terminals, and their function is regulated by auxiliary $\alpha_2\delta$ and β subunits. All four mammalian $\alpha_2\delta$ subunits enhance calcium currents through Ca_V1 and Ca_V2 channels, and this increase is attributed, in part, to increased Ca_V expression at the plasma membrane. In the present study we provide evidence that $\alpha_2\delta$-1, like $\alpha_2\delta$-2, is recycled to the plasma membrane through a Rab11a-dependent endosomal recycling pathway. Using a dominant-negative Rab11a mutant, Rab11a(S25N), we show that $\alpha_2\delta$-1 increases plasma membrane $Ca_V2.2$ expression by increasing the rate and extent of net forward $Ca_V2.2$ trafficking in a Rab11a-dependent manner. Dominant-negative Rab11a also reduces the ability of $\alpha_2\delta$-1 to increase $Ca_V2.2$ expression on the cell-surface of hippocampal neurites. In contrast, $\alpha_2\delta$-3 does not enhance rapid forward $Ca_V2.2$ trafficking, regardless of whether Rab11a(S25N) is present. In addition, whole-cell $Ca_V2.2$ currents are reduced by co-expression of Rab11a(S25N) in the presence of $\alpha_2\delta$-1, but not $\alpha_2\delta$-3. Taken together these data suggest that $\alpha_2\delta$ subtypes participate in distinct trafficking pathways which in turn influence the localisation and function of $Ca_V2.2$.

The Ca_V1 and Ca_V2 voltage-gated calcium channels associate with auxiliary $\alpha_2\delta$ and ß subunits[1]. The $\alpha_2\delta$ subunits are glycosyl-phosphatidylinositol-anchored extracellular proteins[2–4]. There are four known mammalian $\alpha_2\delta$ isoforms ($\alpha_2\delta$-1-4) which are thought to have similar functions and topological features, despite a surprising lack of sequence homology between them[5]. The $\alpha_2\delta$ subunits have long been known to enhance whole-cell currents through Ca_V channels[6–9]. However, to date there is limited evidence that $\alpha_2\delta$s strongly influence single-channel properties of Ca_V channels[8]. As such, $\alpha_2\delta$-mediated enhancement of Ca_V currents has often been attributed primarily to increased channel trafficking and plasma membrane insertion[8,10–13].

The development of functional exofacially-tagged Ca_V2 constructs[10], has allowed us to define populations of plasma membrane-inserted Ca_V2 channels using imaging approaches. This method was previously used to demonstrate that heterologous expression of $\alpha_2\delta$-1 increases cell-surface $Ca_V2.2$ expression, consistent with earlier models of $\alpha_2\delta$-1 function[10]. However, subsequent studies on the proteolytic processing of $\alpha_2\delta$ have found that unprocessed $\alpha_2\delta$-1 is unable to enhance macroscopic Ca_V currents despite increasing cell-surface $Ca_V2.2$ expression in cell lines[14,15]. These studies provide convincing evidence that the $\alpha_2\delta$-mediated increase in Ca_V currents is dependent on an increase in cell-surface $Ca_V2.2$ expression, but also requires a molecular activation switch, triggered by the proteolytic cleavage of $\alpha_2\delta$ into α_2 and δ. Presently, it is unclear whether $\alpha_2\delta$ isoforms differ significantly in their ability to enhance Ca_V currents, and it remains to be seen if $\alpha_2\delta$ subtypes have uniform trafficking mechanisms particularly with regard to their effect on Ca_V localisation.

In a previous study[16], we found that the cell-surface localization of $\alpha_2\delta$-2, following its heterologous expression, was increased by recycling from Rab11a-dependent endosomes back to the plasma membrane. Rab11a belongs to the Rab family of small GTPases which regulate a multitude of intracellular trafficking pathways, facilitating membrane targeting, cargo sorting and vesicle fusion events through recruitment of effectors and direct interactions with cargo proteins[17]. Rab11 proteins are particularly involved in trafficking through recycling endosomes[18,19], and inhibition of Rab11a-dependent recycling can be achieved through expression of the dominant-negative mutant Rab11a(S25N), which is locked in an inactive GDP-bound conformation[20]. Cell-surface expression of $\alpha_2\delta$-2 is reduced in the presence of Rab11a(S25N)[16], and this occludes the effect of the $\alpha_2\delta$ ligand gabapentin, which itself reduces cell-surface expression of $\alpha_2\delta$-1 and $\alpha_2\delta$-2[11,16]. These data provide a mechanistic

Department of Neuroscience, Physiology and Pharmacology, University College London, Gower Street, London WC1E 6BT, UK. ✉email: a.dolphin@ucl.ac.uk

explanation for the action of gabapentin, whereby $\alpha_2\delta$ bound to gabapentin is prevented from recycling to the plasma membrane via Rab11-positive endosomes, resulting in a loss of $\alpha_2\delta$ cell-surface expression[16]. Mutational studies have revealed that gabapentin acts by binding to a site including an RRR motif in the α_2 domain, which is present in $\alpha_2\delta$-1 and $\alpha_2\delta$-2[21–24]. However, since $\alpha_2\delta$-3 is also widely distributed in the nervous system, if there were functional differences, for example between $\alpha_2\delta$-1 and $\alpha_2\delta$-3, this might influence the trafficking and localisation of associated Ca_V channels.

In the present study, we wished to determine to what extent the enhancement of plasma membrane $Ca_V2.2$ expression, a previously-demonstrated feature of $\alpha_2\delta$-1 function, is conserved for $\alpha_2\delta$-3. We then sought to elucidate further the mechanisms through which $\alpha_2\delta$s increase cell-surface $Ca_V2.2$, and to understand how this process influences the localization and function of $Ca_V2.2$ in cell lines and hippocampal neurons. We find that $\alpha_2\delta$ subunits have a differential effect on $Ca_V2.2$ trafficking; although all $\alpha_2\delta$ proteins tested increase $Ca_V2.2$ cell-surface expression to varying extents, only $\alpha_2\delta$-1 and $\alpha_2\delta$-2 rapidly increase net forward trafficking of $Ca_V2.2$; by contrast $\alpha_2\delta$-3 does not influence this process, within a 45-min time-frame. Further examination showed that the enhanced forward trafficking of $Ca_V2.2$ is a Rab11a-dependent effect and that $\alpha_2\delta$-1 and $\alpha_2\delta$-2 participate in Rab11a-dependent recycling, whereas $\alpha_2\delta$-3 does not.

Results

Rab11a-dependent recycling affects $\alpha_2\delta$-1 but not $\alpha_2\delta$-3 cell-surface expression. Trafficking through Rab11a-positive recycling endosomes enhances $\alpha_2\delta$-2 membrane expression, a pathway that is inhibited by gabapentin[16]. The α_2 domain of both $\alpha_2\delta$-1 and $\alpha_2\delta$-2 contains a triple RRR motif, the third R of which is required for gabapentin binding, and is absent from the $\alpha_2\delta$-3 and $\alpha_2\delta$-4 sequences[12,25]. Here, we considered the possibility that $\alpha_2\delta$-1 and $\alpha_2\delta$-2 enhance cell-surface $Ca_V2.2$ expression, at least in part, by facilitating the recycling of $Ca_V2.2$ through Rab11a-positive endosomes. Further to this, we speculated that $\alpha_2\delta$-3 may traffic independently of this pathway.

To test this hypothesis, we have used the dominant-negative Rab11a(S25N) mutant, which we found previously to inhibit cell-surface expression of $\alpha_2\delta$-2[16], and thus a similar result was expected for $\alpha_2\delta$-1. In our previous study[16] we found no effect of co-expressing WT Rab11a on any aspects of $\alpha_2\delta$ trafficking or calcium channel function, and thus it was not included as an additional control in the present study. We compared cell-surface expression of HA-tagged $\alpha_2\delta$-1 and $\alpha_2\delta$-3, in the absence and presence of Rab11a(S25N) (Fig. 1A,B). Cell-surface $\alpha_2\delta$-3 immunostaining is typically weaker than that for $\alpha_2\delta$-1 (Fig. 1A), so we used antigen retrieval to maximise available HA signal. We found a reduction in cell-surface $\alpha_2\delta$-1-HA staining of 47%, when co-expressed with Rab11a(S25N) (Fig. 1B). In contrast $\alpha_2\delta$-3 showed no significant difference in cell-surface expression whether expressed with or without Rab11a(S25N) (Fig. 1B). These data provide evidence that $\alpha_2\delta$-1, like $\alpha_2\delta$-2[16], is regulated by Rab11a-dependent recycling and suggest that cell-surface expression of $\alpha_2\delta$-3 is not promoted by trafficking through this endosomal recycling pathway (Fig. 1D). This result was supported by measurement of the intracellular $\alpha_2\delta$ levels which were strongly reduced by Rab11a(S25N) in the case of $\alpha_2\delta$-1 but not $\alpha_2\delta$-3 (Fig. 1A,C). This suggests that block of recycling endosome function may lead re-routing of $\alpha_2\delta$-1 to degradation pathways (Fig. 1D), although this will require further experimentation.

Cell-surface $Ca_V2.2$ expression is reduced by Rab11a(S25N) when $\alpha_2\delta$-1 or $\alpha_2\delta$-2 are present. In our previous study[16], we found that inhibition of $\alpha_2\delta$-2 recycling through Rab11a-positive endosomes reduced whole-cell $Ca_V2.2$ currents. However, a direct effect on plasma membrane insertion of associated Ca_V channels was not examined. Here we compared the plasma membrane expression of exofacially-tagged $Ca_V2.2$, containing a bungarotoxin binding site (BBS) tag[10], when co-expressed with ß1b, either alone or together with $\alpha_2\delta$-1, or $\alpha_2\delta$-3. We then examined the effect of Rab11a(S25N) (Fig. 2A). Plasma membrane-inserted $Ca_V2.2$ was increased by 92% and 38% when co-expressed with $\alpha_2\delta$-1 and $\alpha_2\delta$-3, respectively (Fig. 2B), in agreement with our previous study[14]. However, Rab11a(S25N) co-expression reduced the plasma membrane level of $Ca_V2.2$ by 53% when $\alpha_2\delta$-1 was present, but had no effect in the presence of $\alpha_2\delta$-3, or in the absence of $\alpha_2\delta$ (Fig. 2B). Total $Ca_V2.2$ levels were also reduced by Rab11a(S25N) in the presence of $\alpha_2\delta$-1 but not in the absence of $\alpha_2\delta$ or presence of $\alpha_2\delta$-3 (Fig. 2A,C). Following these findings, we also compared the effect of Rab11a(S25N) on plasma membrane $Ca_V2.2$ in the presence $\alpha_2\delta$-2 (Fig. S1A,B). As expected, cell-surface $Ca_V2.2$ expressed with $\alpha_2\delta$-2 and β1b was reduced by 35% by Rab11a(S25N) (Fig. S1B).

Together, these data suggest that $\alpha_2\delta$-1 and $\alpha_2\delta$-2 enhance cell-surface $Ca_V2.2$ expression, in part through Rab11a-dependent recycling to the plasma membrane, which $Ca_V2.2$ is unable to access independently of these $\alpha_2\delta$ subunits. In contrast, although $\alpha_2\delta$-3 produced a 38% increase in $Ca_V2.2$ cell-surface expression (Fig. 2B), this was independent of a Rab11a-dependent recycling pathway, suggesting that $\alpha_2\delta$-3 is only able to promote cell-surface $Ca_V2.2$ trafficking through another pathway, such as direct trafficking from the Golgi apparatus.

Rab11a(S25N) reduces $Ca_V2.2$ expression in neurites of cultured hippocampal neurons when co-expressed with $\alpha_2\delta$-1 but not $\alpha_2\delta$-3. We have previously demonstrated that Ca_Vß subunits are able to increase plasma membrane expression of $Ca_V2.2$ in non-neuronal cells, even in the absence of $\alpha_2\delta$, although there is generally an approximately twofold increase in the presence of $\alpha_2\delta$-1[10,14] (see Fig. 2B). However, in primary hippocampal neuronal cultures, we have found the presence of $\alpha_2\delta$ to be critical for localisation of $Ca_V2.2$ to neurites[14]. Here, we examined whether $Ca_V2.2$ expression on the surface of hippocampal neurites is also influenced by Rab11a in an $\alpha_2\delta$-dependent manner. To do this we used an exofacially HA-tagged and N-terminally GFP-tagged $Ca_V2.2$ construct[26], which allowed us to quantify cell-surface and total $Ca_V2.2$ expression in non-permeabilised neurons. We expressed GFP-$Ca_V2.2$-HA plus β1b, with or without $\alpha_2\delta$-1 or $\alpha_2\delta$-3, and with or without Rab11a(S25N) (Fig. 3A). In accordance with our previous studies[14], expression of $Ca_V2.2$

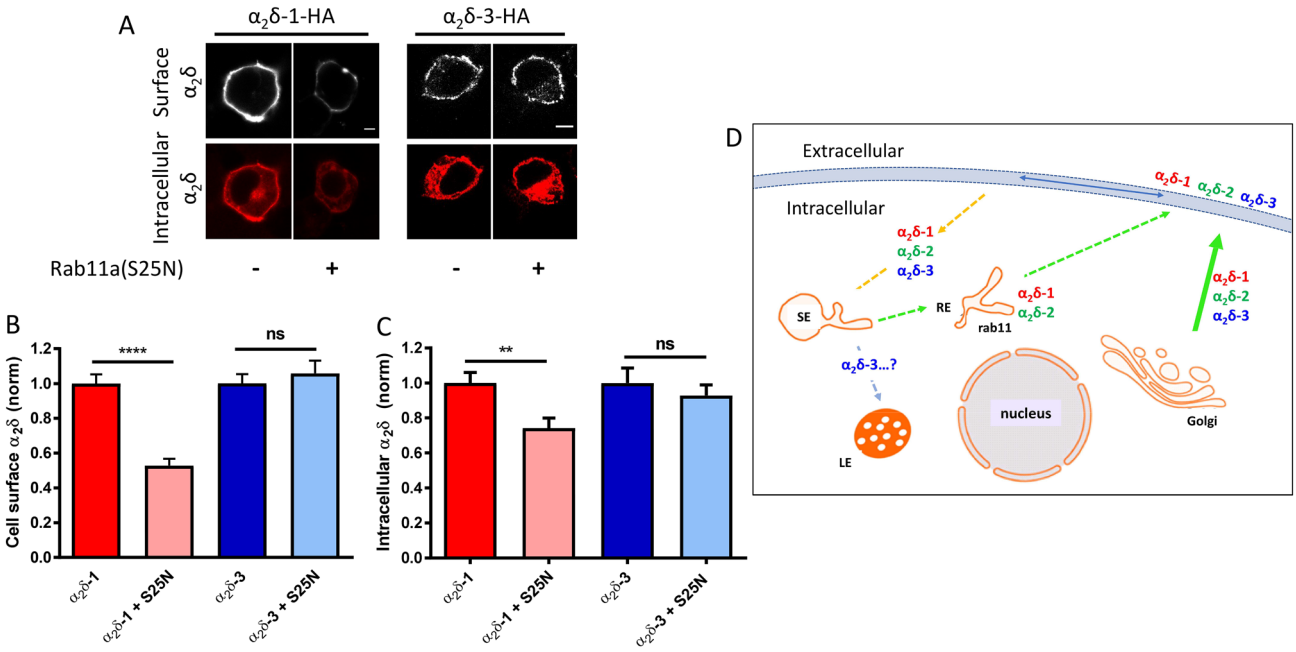

Figure 1. Dominant-negative Rab11a(S25N) reduces steady-state cell-surface expression of HA-tagged $\alpha_2\delta$-1 but not $\alpha_2\delta$-3. (**A**) Confocal images of cell-surface (top row) and intracellular (bottom row) HA staining in N2a cells expressing $\alpha_2\delta$-1-HA (left) or $\alpha_2\delta$-3-HA (right) in the absence or presence of Rab11a(S25N). Scale bars (5 µm) refer to either $\alpha_2\delta$-1 or $\alpha_2\delta$-3 expressing cells. Cell surface HA was detected in non-permeabilised cells and intracellular HA subsequently detected following permeabilization (see Methods). (**B**) Normalized mean cell-surface $\alpha_2\delta$ expression for $\alpha_2\delta$-1 control (red), $\alpha_2\delta$-1 + Rab11a(S25N) (pink), $\alpha_2\delta$-3 control (blue), $\alpha_2\delta$-3 + Rab11a(S25N) (light blue). (**C**) Normalized mean intracellular $\alpha_2\delta$ expression for $\alpha_2\delta$-1 control (red), $\alpha_2\delta$-1 + Rab11a(S25N) (pink), $\alpha_2\delta$-3 control (blue), $\alpha_2\delta$-3 + Rab11a(S25N) (light blue). For (**B**) and (**C**), mean fluorescence intensity per cell was normalized to mean $\alpha_2\delta$ control conditions for each experiment. Normalised data were then pooled from 3 separate experiments and plotted as mean ± SEM. Each cell was measured for cell-surface and intracellular HA expression: $\alpha_2\delta$-1 control (n = 159 cells), $\alpha_2\delta$-1 + Rab11a(S25N) (n = 161 cells), $\alpha_2\delta$-3 control (n = 134 cells), $\alpha_2\delta$-3 + Rab11a(S25N) (n = 135 cells). Statistical significance was determined using Student's unpaired t test with Welch's correction; **, $P = 0.0022$; ****, $P < 0.0001$. (**D**) Diagram of pathways for $\alpha_2\delta$ membrane expression and recycling, and Rab11 expression. SE = sorting endosome, RE = recycling endosome, LE = late endosome/lysosome. Dotted pathways represent hypothetical routes.

on the cell-surface of neurites (which had the appearance of dendrites, see Methods) was extremely low in the absence of $\alpha_2\delta$ (Fig. 3A,B), and we found no effect of co-expression of Rab11a(S25N) on this. We observed a ~ fourfold increase in cell-surface $Ca_V2.2$-HA expression with $\alpha_2\delta$-1, and ~ 3.5-fold increase with $\alpha_2\delta$-3, relative to control (Fig. 3B). Expression of GFP in the neurites, representing total $Ca_V2.2$, was also elevated by co-expression of both $\alpha_2\delta$-1 and $\alpha_2\delta$-3, by 2.1-fold and 1.9-fold, respectively (Fig. 3C). Consistent with our findings in non-neuronal cells, cell-surface $Ca_V2.2$-HA was reduced by co-expression of Rab11a(S25N) in the presence of $\alpha_2\delta$-1 (by ~ 44%), but was not affected in the presence of $\alpha_2\delta$-3 (Fig. 3B). However, we saw no change in total $Ca_V2.2$-GFP expression in the neurites with Rab11a(S25N), either in the absence or presence of $\alpha_2\delta$-1 or $\alpha_2\delta$-3 (Fig. 3C). Together these data suggest that Rab11a-dependent recycling enhances neurite $Ca_V2.2$ cell-surface expression in an $\alpha_2\delta$-selective manner.

Rab11a(S25N) reduces whole-cell $Ca_V2.2$ currents when co-expressed with $\alpha_2\delta$-1 but not $\alpha_2\delta$-3. Here we investigated whether the reduction in cell-surface $Ca_V2.2$ expression by Rab11a(S25N) correlates to a change in whole-cell Ca_V currents and whether any change we observe is $\alpha_2\delta$-dependent. We used patch-clamp recording to measure whole-cell Ba^{2+} currents in tsA201 cells expressing $Ca_V2.2/\beta1b/\alpha_2\delta$, with or without Rab11a(S25N) (Fig. 4A). We found that the peak Ba^{2+} current density was reduced by 59% at + 10 mV, when $\alpha_2\delta$-1 and Rab11a(S25N) were co-expressed, compared to $\alpha_2\delta$-1 expressed alone (Fig. 4A,B). Corresponding maximum conductance (G_{max}) values were reduced from 1.4 ± 0.2 to 0.7 ± 0.1 nS/pF by the presence of Rab11a(S25N) (Fig. 4C). We saw no significant changes to steady-state inactivation under the two conditions (Fig. S2A), supporting the view that current density changes occurred as a result of reduced plasma membrane $Ca_V2.2$ expression rather than changes to biophysical properties of the channels.

Having established that Rab11a(S25N) reduced both $\alpha_2\delta$-1-mediated $Ca_V2.2$ plasma membrane expression and $Ca_V2.2$ current enhancement to similar extents, it was necessary to determine whether Rab11a(S25N) would produce a reduction in $\alpha_2\delta$-3-mediated $Ca_V2.2$ current enhancement. In contrast with the effect of $\alpha_2\delta$-1, we found no difference in mean current density (Fig. 4D,E), G_{max} (Fig. 4F) or steady-state inactivation (Fig. S2B) when Rab11a(S25N) was co-expressed with $\alpha_2\delta$-3, compared to $\alpha_2\delta$-3 alone. This result is consistent with our

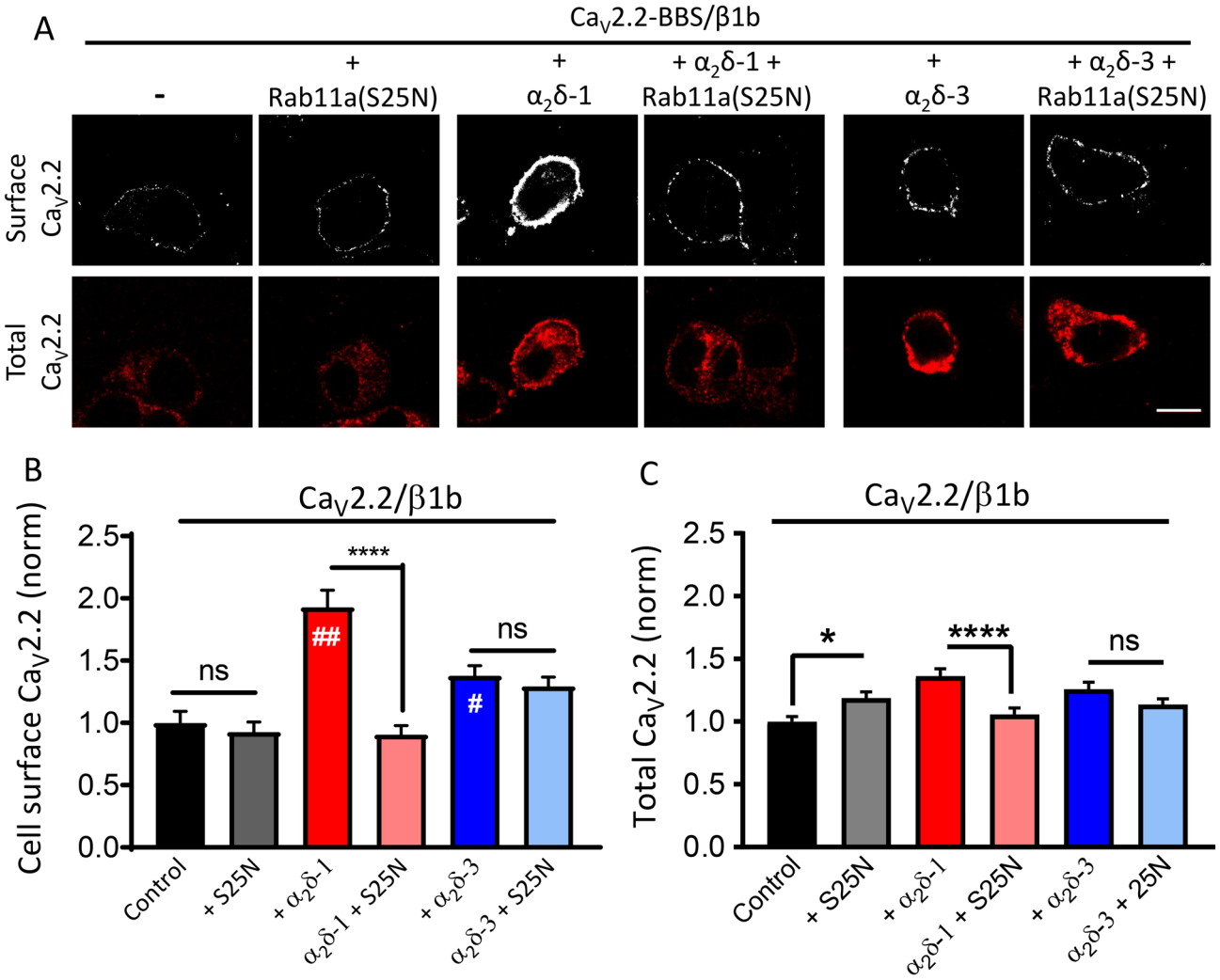

Figure 2. Steady-state cell-surface $Ca_V2.2$ is reduced by Rab11a(S25N) when expressed with $\alpha_2\delta$-1, but not $\alpha_2\delta$-3. (**A**) Confocal images of cell-surface (top row, BBS, live-labelled with α-BTX) and total (bottom row, II-III loop Ab) $Ca_V2.2$-BBS expressed in N2a cells with β1b and either: no $\alpha_2\delta$, $\alpha_2\delta$-1, or $\alpha_2\delta$-3, in the absence or presence of Rab11a(S25N). Scale bar applies to all images = 5 µm. (**B**) Mean cell-surface $Ca_V2.2$-BBS levels expressed in N2a cells with β1b and: no $\alpha_2\delta$ (black, n = 142), no $\alpha_2\delta$ + Rab11a(S25N) (grey, n = 145 cells), $\alpha_2\delta$-1 (red, n = 148 cells), $\alpha_2\delta$-1 + Rab11a(S25N) (pink, n = 140 cells), $\alpha_2\delta$-3 (blue, n = 132 cells), $\alpha_2\delta$-3 + Rab11a(S25N) (light blue, n = 144 cells), normalized to the control level in the absence of $\alpha_2\delta$. Statistical significance was determined using one-way ANOVA ($F = 17.72$, $P < 0.0001$) and Sidak's multiple comparison post hoc tests; ns, $P = 0.986$ for control, $P = 0.975$ for $\alpha_2\delta$-3; ****, $P < 0.0001$; ##, $P < 0.0001$ vs no $\alpha_2\delta$; #, $P = 0.0213$ vs no $\alpha_2\delta$. (**C**) Total $Ca_V2.2$-BBS in cells shown in (B). Statistical significance was determined using one-way ANOVA ($F = 6.752$, $P < 0.0001$) and Sidak's multiple comparison tests; ns, $P = 0.284$; *, $P = 0.0302$; ***, $P < 0.0001$. For (**B**) and (**C**), each cell was measured for cell-surface BBS expression in non-permeabilised cells using α-BTX-AF488, and for total $Ca_V2.2$ following permeabilization using the II-III loop Ab (see Methods). Fluorescence intensity per cell was normalized to mean $Ca_V2.2$/β1b control condition for each experiment. Normalized data were then pooled from 3 separate experiments and plotted ± SEM.

observation that cell-surface expression of $Ca_V2.2$ is unaffected by Rab11a-dependent recycling when expressed with $\alpha_2\delta$-3.

Net forward trafficking of $Ca_V2.2$ is enhanced by $\alpha_2\delta$-1 and $\alpha_2\delta$-2, but not $\alpha_2\delta$-3. Having provided evidence that $\alpha_2\delta$-3 enhances steady-state plasma membrane $Ca_V2.2$ expression, albeit to a smaller degree than $\alpha_2\delta$-1 (Fig. 2B), we considered two possible explanations for this effect: (1) $\alpha_2\delta$ subunits increase forward trafficking of $Ca_V2.2$ to the cell-surface, or (2) $\alpha_2\delta$ subunits reduce the rate of $Ca_V2.2$ endocytosis from the cell-surface. Previously, we found that the rate of $Ca_V2.2$ endocytosis was not altered by expression of $\alpha_2\delta$-1[10,27]. In the present study, we used an α-bungarotoxin (BTX) live-labelling approach to compare the rates of net forward trafficking of $Ca_V2.2$-BBS expressed with β1b either alone or together with $\alpha_2\delta$-1, $\alpha_2\delta$-2 or $\alpha_2\delta$-3 (Fig. 5A). When compared to control conditions, we found that co-expression of $\alpha_2\delta$-1 and $\alpha_2\delta$-2 produced significantly higher insertion of $Ca_V2.2$ into the plasma membrane, at each time point tested, starting at 15 min (Fig. 5B). In contrast,

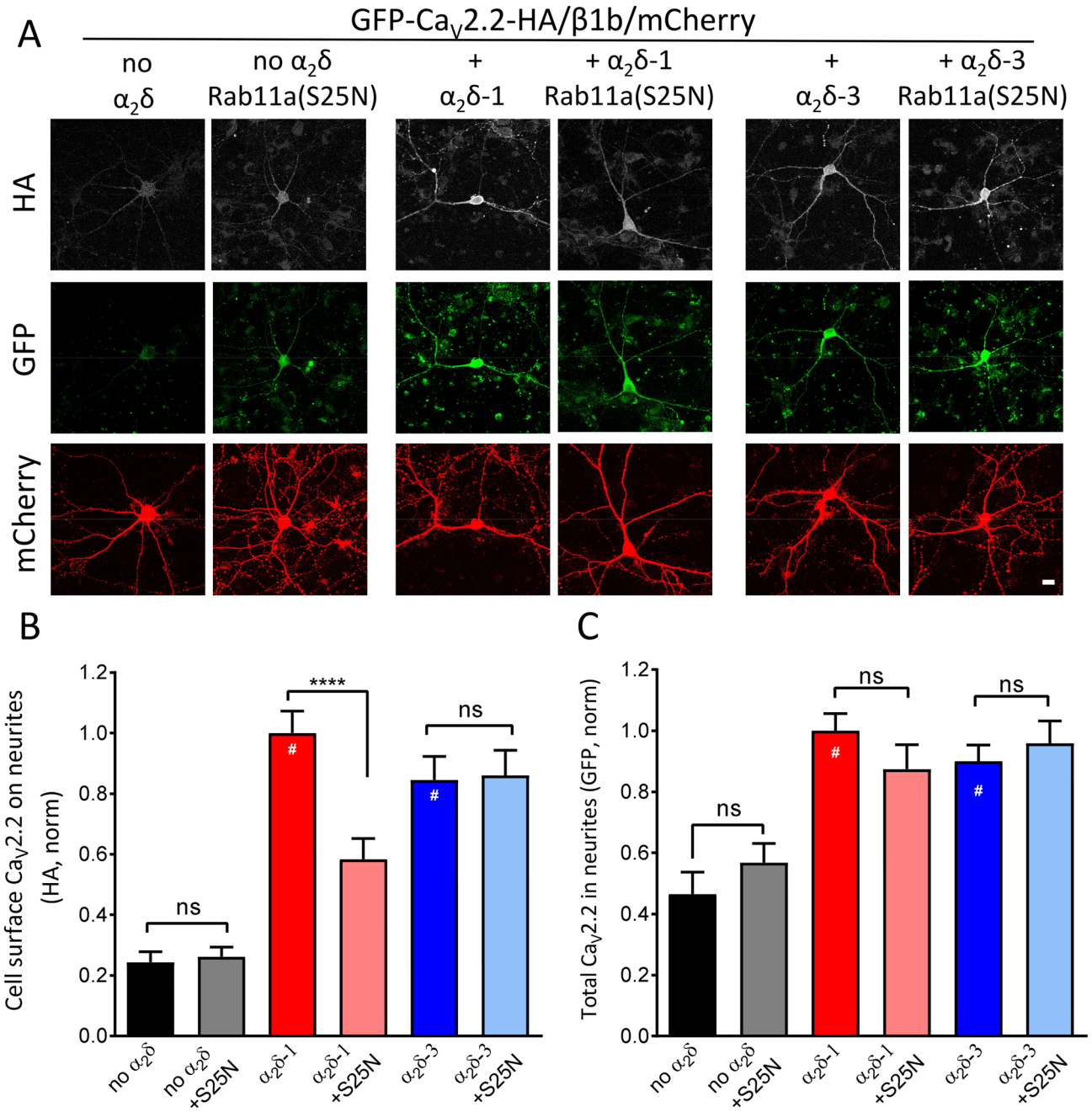

Figure 3. Rab11a(S25N) reduces plasma membrane-inserted $Ca_V2.2$ in hippocampal neurites when expressed with $\alpha_2\delta$-1 but not without $\alpha_2\delta$ or with $\alpha_2\delta$-3. (**A**) Confocal images of rat hippocampal pyramidal neurons expressing GFP-$Ca_V2.2$-HA/β1b/mCherry control, + Rab11a(S25N), $\alpha_2\delta$-1, $\alpha_2\delta$-1 + Rab11a(S25N), $\alpha_2\delta$-3 or $\alpha_2\delta$-3 + Rab11a(S25N). Scale bar applies to all images = 20 µm. Top row, HA immunostaining in non-permeabilised neurons to measure cell surface $Ca_V2.2$; middle row, GFP to determine total $Ca_V2.2$ expression; bottom row, mCherry (transfection marker) expression. (**B**) Normalized mean cell-surface GFP-$Ca_V2.2$-HA, determined from HA staining in non-permeabilised neurons, in the processes of pyramidal rat neurons expressed with β1b/mCherry for control (black), Rab11a(S25N) (grey), $\alpha_2\delta$-1 (red), $\alpha_2\delta$-1 + Rab11a(S25N) (pink), $\alpha_2\delta$-3 (blue) or $\alpha_2\delta$-3 + Rab11a(S25N) (light blue). Statistical significance was determined using one-way ANOVA ($F = 16.32$, $P < 0.0001$) and Sidak's multiple comparison post hoc tests; ns, $P > 0.999$ for both control vs S25N and $\alpha_2\delta$-3 vs $\alpha_2\delta$-3 + S25N; ****, $P < 0.0001$. Significance vs no $\alpha_2\delta$ control: #, $P < 0.0001$ for both $\alpha_2\delta$-1 and $\alpha_2\delta$-3. (**C**) Normalized mean total GFP-$Ca_V2.2$-HA (determined from GFP density) in the processes of pyramidal rat neurons expressed with β1b/mCherry for control (black), Rab11a(S25N) (grey), $\alpha_2\delta$-1 (red), $\alpha_2\delta$-1 + Rab11a(S25N) (pink), $\alpha_2\delta$-3 (blue) or $\alpha_2\delta$-3 + Rab11a(S25N) (light blue). Statistical significance was determined using one-way ANOVA ($F = 8.74$, $P < 0.0001$) and Sidak's multiple comparison post hoc tests; ns, $P = 0.925$ for control vs S25N; $P = 0.559$ for $\alpha_2\delta$-1 vs $\alpha_2\delta$-1 + S25N; $P = 0.974$ for $\alpha_2\delta$-3 vs $\alpha_2\delta$-3 + S25N. Significance vs no $\alpha_2\delta$ control: #, $P < 0.0001$ for both $\alpha_2\delta$-1 and $\alpha_2\delta$-3. For (**B**) and (**C**), between 2–5 neuronal processes were measured and averaged per cell, 10–15 cells per condition per experiment, for a total of 3 transfections. Total cell numbers for each condition: control (n = 30 cells), Rab11a(S25N) (n = 19 cells), $\alpha_2\delta$-1 (n = 51 cells), $\alpha_2\delta$-1 + Rab11a(S25N) (n = 42 cells), $\alpha_2\delta$-3 (n = 46) and $\alpha_2\delta$-3 + Rab11a(S25N) (n = 40 cells). Normalized mean fluorescence intensity per neuron was pooled from three separate experiments and data are plotted ± SEM values.

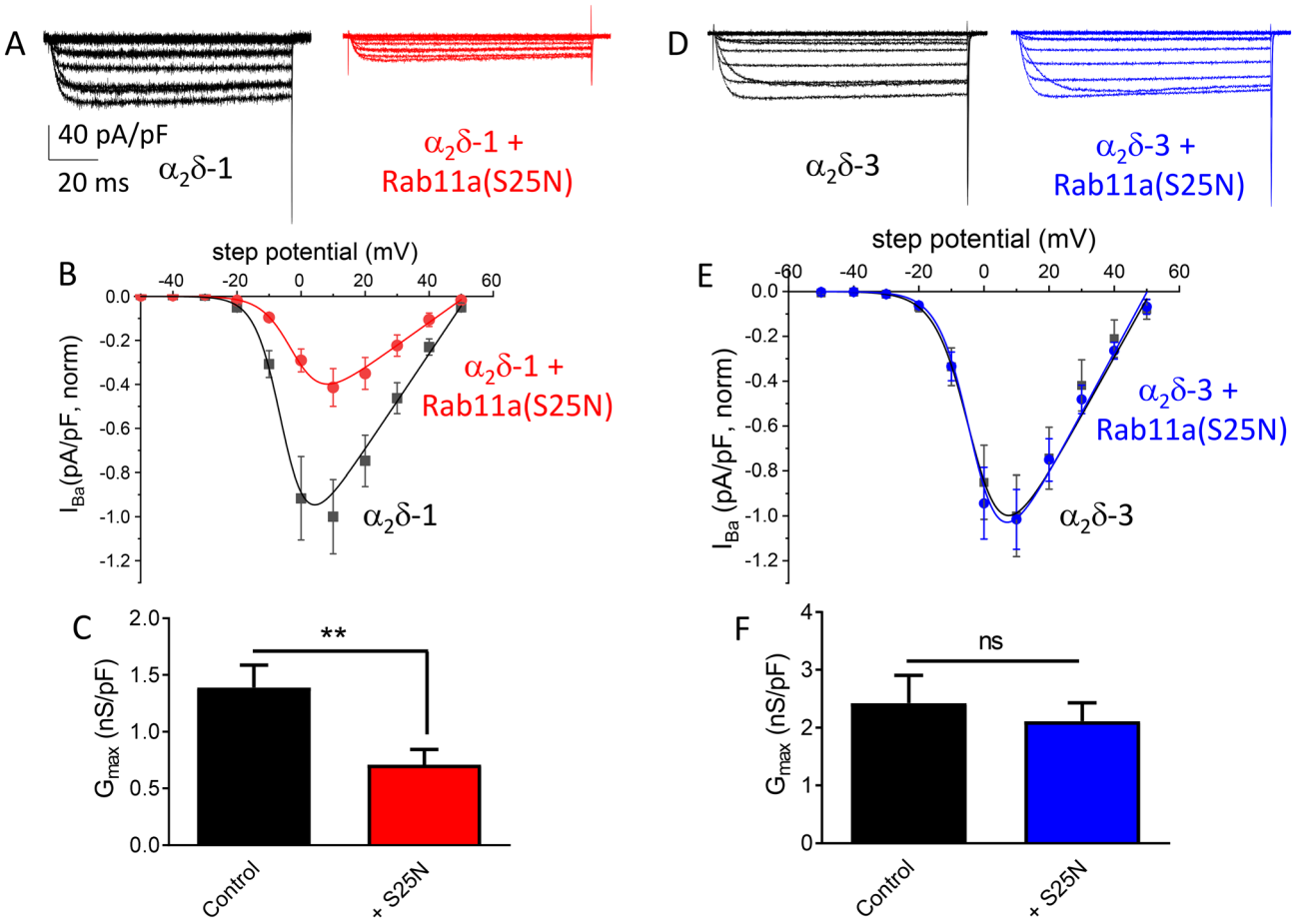

Figure 4. Rab11a(S25N) reduces whole-cell $Ca_V2.2$ currents when expressed with $\alpha_2\delta$-1, but not $\alpha_2\delta$-3. (**A**) Example whole-cell current traces for $Ca_V2.2$ expressed in tsA-201 cells with: β1b/$\alpha_2\delta$-1 (black) and β1b/$\alpha_2\delta$-1 + Rab11a(S25N) (red). Scale bars (40 pA/pF and 20 ms) refer to all traces. (**B**) Mean *IV* plots for $Ca_V2.2$ with: β1b/$\alpha_2\delta$-1 (black squares, n = 15) and β1b/$\alpha_2\delta$-1 + Rab11a(S25N) (red circles, n = 14), fitted by a modified Boltzmann function. The potentials for 50% activation were -4.23 ± 0.76 mV, and -1.39 ± 1.26 mV, respectively. (**C**) Mean G_{max} values obtained by fitting each individual trace in (B) to a modified Boltzmann function $Ca_V2.2$/β1b/$\alpha_2\delta$-1 (black), $Ca_V2.2$/β1b/$\alpha_2\delta$-1 + Rab11a(S25N) (red). Statistical significance determined by Student's unpaired t-test; **, $P = 0.0093$. (**D**) Example whole-cell current traces for $Ca_V2.2$ with: β1b/$\alpha_2\delta$-3 (black) and β1b/$\alpha_2\delta$-3 + Rab11a(S25N) (blue). (**E**) Mean *IV* plots for $Ca_V2.2$ with: β1b/$\alpha_2\delta$-3 (black squares, n = 15) and β1b/$\alpha_2\delta$-3 + Rab11a(S25N) (blue circles, n = 14), fitted by a modified Boltzmann function. The potentials for 50% activation were -4.21 ± 1.59 mV and -3.93 ± 0.98 mV, respectively. (**F**) Mean G_{max} values obtained by fitting each individual trace in (**E**) to a modified Boltzmann function $Ca_V2.2$/β1b/$\alpha_2\delta$-3 (black), $Ca_V2.2$/β1b/$\alpha_2\delta$-3 + Rab11a(S25N) (blue). Data are plotted as mean ± SEM. Statistical significance determined by Student's unpaired t-test; ns, $P = 0.5816$.

the appearance of $Ca_V2.2$ on the cell-surface did not differ significantly between the control and $\alpha_2\delta$-3 conditions up to 45 min, but there was a statistically significant increase of 23% at 60 min (Fig. 5B), which is consistent with our observation of its effect on steady-state $Ca_V2.2$ expression (Fig. 2B). Estimates for initial rates of net forward $Ca_V2.2$ trafficking were made using the slope value of a straight line between 0 and 15 min. While there was a 2.7-fold increase in initial rate of $Ca_V2.2$ appearance on the cell-surface with $\alpha_2\delta$-1 co-expression compared to control (Fig. 5C), we found no significant difference in initial $Ca_V2.2$ trafficking rates for the $\alpha_2\delta$-3 condition. Together these data support a role for $\alpha_2\delta$-1 in enhancing rapid plasma membrane-insertion of $Ca_V2.2$ by increasing the rate of forward trafficking, whereas $\alpha_2\delta$-3 had no clear effect on the initial rate of forward $Ca_V2.2$ trafficking (Fig. 5C).

Dominant-negative Rab11a reduces net forward trafficking of $\alpha_2\delta$-1. Next, we compared net forward trafficking rates of $\alpha_2\delta$-1-BBS in the presence or absence of Rab11a(S25N) (Fig. 6A). We found that net forward trafficking of $\alpha_2\delta$-1-BBS was reduced by co-expression of Rab11a(S25N), with a 41% reduction in cell-surface $\alpha_2\delta$-1-BBS after 30 min (Fig. 6B), consistent with the reduction in cell-surface $\alpha_2\delta$-1-HA induced by Rab11a(S25N) under steady-state conditions (Fig. 1B). We then compared net forward trafficking of $Ca_V2.2$-BBS, when expressed with or without $\alpha_2\delta$-1 and with or without Rab11a(S25N), at two time points, 10 and 30 min (Fig. 6C–E). As expected, $\alpha_2\delta$-1 enhanced net-forward trafficking of $Ca_V2.2$, and Rab11a(S25N) abolished this

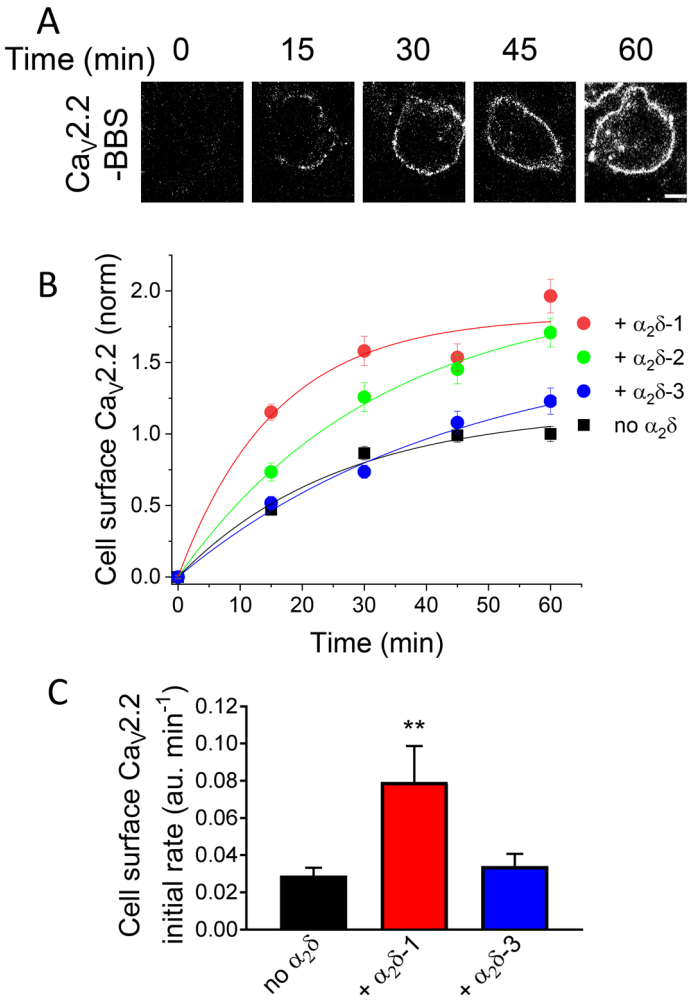

Figure 5. Net forward trafficking of $Ca_V2.2$-BBS is increased by $\alpha_2\delta$-1 and $\alpha_2\delta$-2, but not by $\alpha_2\delta$-3. (**A**) Example images from forward trafficking assay for $Ca_V2.2$-BBS expressed in N2a cells with β1b and $\alpha_2\delta$-1. Cells were live-labelled with α-BTX-AF488 for 0, 15, 30, 45, and 60 min, following pre-incubation with unlabelled α-BTX at 17 °C for 30 min. Scale bar = 5 µm. (**B**) Normalized mean cell-surface $Ca_V2.2$-BBS fluorescence in cells expressing $Ca_V2.2$-BBS and β1b alone (black) or with either $\alpha_2\delta$-1 (red), $\alpha_2\delta$-2 (green) or $\alpha_2\delta$-3 (blue). An average of 30—60 cells were analysed per time point, for each condition in an individual experiment. The data were collected as paired experiments between $Ca_V2.2/\beta1b$ (control) and $Ca_V2.2/\beta1b + \alpha_2\delta$ (n = 3 each), with a total of 9 for $Ca_V2.2/\beta1b$. Individual experiments were normalized to mean 60 min fluorescence of the paired $Ca_V2.2/\beta1b$ condition, before being pooled together. Data were fitted with an exponential association equation; the time constant (τ) = 26.1 min (no $\alpha_2\delta$), 15.6 min (+ $\alpha_2\delta$-1), 32.4 min (+ $\alpha_2\delta$-2) and 44.9 min (+ $\alpha_2\delta$-3) and asymptotic normalized cell-surface $Ca_V2.2$ (amplitude) = 1.17 (no $\alpha_2\delta$), 1.82 (+ $\alpha_2\delta$-1), 2.0 (+ $\alpha_2\delta$-2) and 1.63 (+ $\alpha_2\delta$3). (**C**) Initial rate of net forward $Ca_V2.2$-BBS trafficking. The gradient of straight line between 0–15 min was obtained as an average for each individual experiment and summarised (in a.u. / min), for $Ca_V2.2/\beta1b$ control (black, n = 9), $Ca_V2.2/\beta1b + \alpha_2\delta$-1 (red, n = 3), and $Ca_V2.2/\beta1b + \alpha_2\delta$-3 (blue, n = 3). Data are mean ± SEM. Statistical significance determined by one-way ANOVA (F = 9.333, $P = 0.0036$) and Dunnett's multiple comparison test vs no $\alpha_2\delta$, ** $P = 0.0021$.

increase at both time points. In sum, these data support the conclusion that $\alpha_2\delta$-1 membrane expression is enhanced by forward-trafficking from Rab11a-positive recycling endosomes, and that $Ca_V2.2$ can traffic through this pathway when co-expressed with Rab11a-sensitive $\alpha_2\delta$-1, but not with $\alpha_2\delta$-3 (Fig. 1D).

Discussion

In this study we have shown that $\alpha_2\delta$ subunits differentially enhance plasma membrane expression of $Ca_V2.2$ in both cell lines and primary neuronal cultures, and have implicated Rab11a-dependent recycling in this process. Rab11 proteins are particularly involved in trafficking through recycling endosomes[18,19], and here we inhibited this route through expression of the dominant-negative mutant Rab11a(S25N)[20]. Our data indicate that $\alpha_2\delta$-1 and $\alpha_2\delta$-2 promote both the steady-state cell-surface $Ca_V2.2$ level and net forward trafficking of $Ca_V2.2$ through a Rab11a-dependent mechanism (Fig. 1D). Blockade of this pathway leads to a reduction in cell-surface $Ca_V2.2$

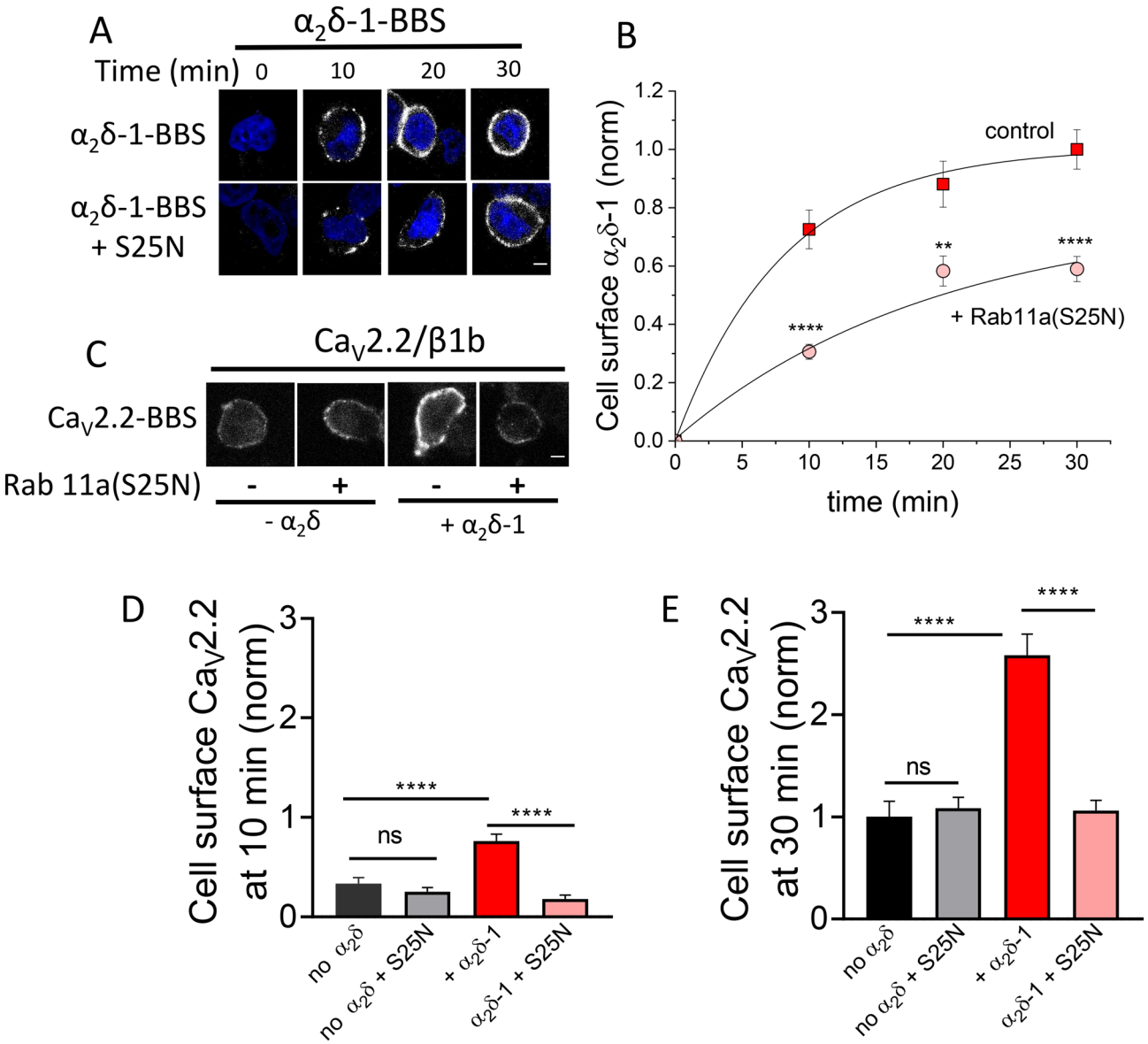

Figure 6. Rab11a(S25N) reduces net forward trafficking of $\alpha_2\delta$-1 and $Ca_V2.2/\beta1b/\alpha_2\delta$-1. (**A**) Confocal images of $\alpha_2\delta$-1-BBS expressed in tsA-201 cells, alone (top row) or with Rab11a(S25N) (bottom row), at each time point of net forward trafficking assay. Cells were live-labelled with α-BTX-AF488 for 0, 10, 20, and 30 min. Nuclei staining with DAPI (blue). Scale bar = 5 µm. (**B**) Net forward $\alpha_2\delta$-1-BBS trafficking, as in (**A**). Normalized mean cell-surface $\alpha_2\delta$-1-BBS expressed either alone (red squares) or with Rab11a(S25N) (pink circles). Data were collected from 3 transfections with approximately 30 to 50 cells analysed per time point in each experiment. Individual experiments were normalized to the $\alpha_2\delta$-1-BBS 30 min time point, before being pooled together. Data were fitted to a single exponential association, with a time constant, $\tau = 8.09$ min for $\alpha_2\delta$-1 control and 19.45 min for $\alpha_2\delta$-1 + Rab11a(S25N). Statistical significance was determined using Student's t test to compare mean fluorescence values between conditions at each time point, ****$P < 0.0001$; **, $P = 0.0018$. (**C**) Confocal images of cell-surface $Ca_V2.2$-BBS expressed in N2a cells with β1b either alone or with $\alpha_2\delta$-1, in the absence or presence of Rab11a(S25N) after 30 min of net forward trafficking assay. Scale bar = 5 µm. (**D,E**) Normalized mean cell-surface $Ca_V2.2$-BBS expressed in N2a cells with β1b and: no $\alpha_2\delta$ (black), no $\alpha_2\delta$ + Rab11a(S25N) (grey), + $\alpha_2\delta$-1 (red) and + $\alpha_2\delta$-1 + Rab11a(S25N) (pink). Cells were live-labelled with α-BTX-AF488 for 10 min (**D**) or 30 min (**E**). Fluorescence intensity per cell was normalized to mean $Ca_V2.2/\beta1b$ controls at 30 min before being pooled from 3 separate experiments and plotted as mean fluorescence ± SEM. For (**D**) no $\alpha_2\delta$ (black, n = 105 cells), no $\alpha_2\delta$ + Rab11a(S25N) (grey, n = 98 cells), + $\alpha_2\delta$-1 (red, n = 123 cells) and + $\alpha_2\delta$-1 + Rab11a(S25N) (pink, n = 112 cells). Statistical significances were determined: using one-way ANOVA ($F = 23.12$, $P < 0.0001$) and Sidak's post hoc tests (**** $P < 0.0001$; ns, $P = 0.672$). For (**E**) no $\alpha_2\delta$ (black, n = 105 cells), no $\alpha_2\delta$ + Rab11a(S25N) (grey, n = 104 cells), + $\alpha_2\delta$-1 (red, n = 132 cells) and + $\alpha_2\delta$-1 + Rab11a(S25N) (pink, n = 118 cells). Statistical significances were determined: using one-way ANOVA ($F = 27.24$, $P < 0.0001$) and Sidak's post hoc tests (**** $P < 0.0001$, ns, $P = 0.975$).

and $\alpha_2\delta$-1 and may lead to increase in degradation, as judged by the reduction in their intracellular levels. However, $\alpha_2\delta$-3 does not appear to participate in the Rab11a-dependent recycling pathway, and does not increase net forward $Ca_V2.2$ trafficking in the short-term (Fig. 5B,C). Despite this, $\alpha_2\delta$-3 consistently increases plasma membrane-inserted $Ca_V2.2$ under steady-state conditions[14]; and the present study, although to a smaller extent than $\alpha_2\delta$-1. Inhibition of Rab11a-dependent recycling also reduces whole-cell $Ca_V2.2$ currents, when expressed with $\alpha_2\delta$-1, but has no effect with $\alpha_2\delta$-3. Our results indicate that one of the main drivers of $\alpha_2\delta$-1-mediated enhancement of $Ca_V2.2$ plasma membrane-insertion is recycling back to the plasma membrane via recycling endosomes. In primary hippocampal neurites, we find that $Ca_V2.2$ membrane expression is largely dependent on $\alpha_2\delta$, and inhibition of Rab11a-dependent recycling also lowers cell-surface $Ca_V2.2$ in neurites in the presence of $\alpha_2\delta$-1. The neurites examined here were of dendritic appearance, 100–150 µm from the soma, and in future it will be of interest to also examine trafficking in axons, because of the differential distribution of $\alpha_2\delta$ subunits in neurons[28,29].

Earlier work from this laboratory has shown that $\alpha_2\delta$-2 participates in recycling through Rab11a-positive recycling endosomes and that this pathway is interrupted by gabapentin[16]. The gabapentin-binding RRR motif is positioned just upstream of the VWA domain in both $\alpha_2\delta$-1 and $\alpha_2\delta$-2, and it has been hypothesised that gabapentinoids displace an endogenous ligand in the binding pocket that includes the RRR motif[11,21,30]. Previous studies using the $\alpha_2\delta$-1(R217A) or $\alpha_2\delta$-2(R282A) mutants, which show much lower affinity for binding gabapentin, found them to have lower ability to enhance Ca_V2 currents compared to their wild-type counterparts, as well as reduced endosomal recycling[11,16,21]. These findings are consistent with the hypothesis that binding of an endogenous ligand in the gabapentin binding site is important for association of $\alpha_2\delta$-1 and $\alpha_2\delta$-2 with endosomal sorting partners. As $\alpha_2\delta$-3 lacks a gabapentin binding site, we hypothesised that it would not participate in Rab11a-dependent recycling and would thereby be unable to promote forward trafficking of $Ca_V2.2$ through this pathway, although the direct route via the Golgi apparatus would still be available[16]. In agreement with this, we find inhibition of Rab11a-dependent recycling did not influence $\alpha_2\delta$-3 trafficking, unlike for $\alpha_2\delta$-1 or $\alpha_2\delta$-2. Presently it is unclear why $\alpha_2\delta$-3 does not participate in Rab11a-dependent recycling, although $\alpha_2\delta$-3 shares only 25.7% sequence homology with $\alpha_2\delta$-1 (ClustalO), which may result in conformational differences that preclude an interaction with a Rab11a effector.

Since Rab11a is a membrane-associated cytoplasmic protein, and $\alpha_2\delta$-1 is extracellular and therefore present in the lumen of recycling endosomes, any functional interaction between the two will involve other proteins. There are several studies that have examined the interaction of $\alpha_2\delta$s with other proteins; for review see[31]. For example, we have demonstrated an interaction between $\alpha_2\delta$-1 and Low-Density Lipoprotein (LDL) Receptor-related Protein-1 (LRP1), a multifunctional receptor which mediates cargo trafficking. LRP1 and its chaperone Rap, promote $\alpha_2\delta$-1 maturation and trafficking to the cell-surface, and also enhance $Ca_V2.2$ currents[32]. Since LRP1 has multiple intracellular and extracellular protein ligands, and contains several cytoplasmic adaptor protein binding motifs[33], it may play a role in $\alpha_2\delta$-1 trafficking via recycling endosomes.

In another study, neurexin-1α enhanced $Ca_V2.1$ currents when expressed with $\alpha_2\delta$-1 but had no effect in the presence of $\alpha_2\delta$-3[34], although no selective and specific interaction with neurexin-1α could be demonstrated, in contrast to a previous study[35]. $\alpha_2\delta$-1 has also been reported to interact with thrombospondins (TSPs) 1–4, which are extracellular matrix proteins[36]. More recently, another study[37] showed a weak interaction between $\alpha_2\delta$-1 and TSP4, but was unable to demonstrate any interaction between cell-surface expressed $\alpha_2\delta$-1 and TSP4, concluding that $\alpha_2\delta$-1 and TSP4 may only interact intracellularly at high concentrations. A further study showed a low affinity interaction between $\alpha_2\delta$-1 and TSP4, but not other TSPs[38]. However, any interaction of $\alpha_2\delta$ subunits with TSPs is unlikely to be involved in their Rab11-dependent recycling.

A number of studies have also linked Rab11a function to growth cone development[39–41]. Since we have demonstrated distinct trafficking pathways for $\alpha_2\delta$-1 and $\alpha_2\delta$-2 compared to $\alpha_2\delta$-3 in relation to Rab11a-dependent recycling, it is possible that other demonstrated subtype-specific functions of $\alpha_2\delta$ proteins[28,42] may also involve distinct trafficking pathways.

Materials and methods

Molecular biology. The following cDNAs were used: $Ca_V2.2$ (rabbit, D14157), $Ca_V2.2$-HA and $Ca_V2.2$-BBS[10], GFP-$Ca_V2.2$-HA[26], β1b (rat, X61394)[43], $\alpha_2\delta$-1 (rat, M86621)[44], $\alpha_2\delta$-1-HA[12,45], $\alpha_2\delta$-1-BBS, in which the BBS tag from $\alpha_2\delta$-2[16] was inserted into $\alpha_2\delta$-1 in the same position as the HA tag, $\alpha_2\delta$-3 (AJ010949), $\alpha_2\delta$-3-HA[14]. mCherry[46] or CD8[47] were included as a transfection markers where stated. Human Rab11a (AF000231) containing the S25N mutation[16,48], was obtained from From Prof. T. Hébert, McGill University.

Antibodies and other materials. Antibodies (Abs) used were: anti-HA Ab (rat monoclonal, Roche), anti-$Ca_V2.2$ II-III loop Ab (rabbit polyclonal)[49]. The following secondary Abs (raised in goat) were used: anti-rat or anti-rabbit IgG-Alexa Fluor (AF) 488 or 594 (ThermoFisher), biotin-labelled anti-rat IgG (Sigma). Other reagents used were BTX-AF488 (Invitrogen) and streptavidin-AF633 (Invitrogen).

Cell lines: culture and transfection. tsA-201 cells were grown in Dulbecco's Modified Eagle Medium (DMEM) (Invitrogen) supplemented with 10% Foetal Bovine Serum, 50 U/ml penicillin/streptomycin and 1% GlutaMAX (Invitrogen). Cells were maintained in tissue culture flasks at 37 °C in a humidified atmosphere of 5% CO_2 and grown up to 70–90% confluence prior to transfection or further passage. Neuro2a (N2a) cells were cultured in 50% DMEM (with high glucose and L-glutamine) and 50% Opti-MEM (with L-glutamine), supplemented with 50 U/ml penicillin/streptomycin, 5% FBS, and 1% GlutaMAX (Life Technologies). The N2a cells were cultured to 80% confluence in a 5% CO_2 incubator at 37 °C and passaged every 3 to 4 d.

For transient expression, N2a or tsA-201 cells were transfected using either PolyJet (SignaGen Laboratories) or Fugene 6 (Promega) in a 3:1 ratio with cDNA mix, according to the manufacturers' instructions. A typical cDNA mix was 2 µg total DNA per 35 mm culture dish at a molar ratio of 3:2:2 of $Ca_V2.2$: β1b: $\alpha_2\delta$. In experiments using Rab11a(S25N) the cDNA mix was 3:2:2:1 for $Ca_V2.2$: β1b: $\alpha_2\delta$: Rab11a(S25N). In conditions lacking a given construct, the DNA mix was supplemented with the appropriate empty vector to have the same total DNA. For fluorescence imaging experiments in either tsA-201 or N2a cells, all cDNAs were in a pcDNA3, pRK5 or pCMV vector. In electrophysiological experiments using tsA-201 cells, all cDNAs were in a pMT2 vector, with the exception of Rab11a(S25N) (pCMV).

Hippocampal neuronal culture and transfection. Hippocampal neurons were isolated from the hippocampus of P0 rats, which were killed under a UK Home Office Schedule 1 procedure. The cerebrum was cut into two, and the hippocampi were extracted from each hemisphere in ice cold HBSS with 10 mM HEPES. The hippocampi were then cut into small segments and digested gently in Papain solution (7 U/ml Papain, 0.2 mg/ml L-Cysteine, 0.2 mg/ml Bovine Serum Albumin (BSA), 5 mg/ml glucose, 10 mM HEPES in HBSS with 30 Kunitz/ml DNase) in a shaking water bath for 40 min at 37 °C. The cells were washed twice with the growth medium (Neurobasal, 2% B27 supplement, 1 unit/ml penicillin, 1 µg/ml streptomycin, 1% GlutaMAX, 0.1% β-mercaptoethanol), and triturated gently. The cells were plated onto 18 mm circular coverslips that are coated with poly-L-lysine and laminin at 750 cells/µl, 100 µl per coverslip. The entire growth medium was changed after 2 h of plating, and half of the medium was then changed every 3–4 d.

Hippocampal neurons were transfected after 7 d in culture, using cDNAs cloned into pCAGGS[50]. 2 h prior to transfection, the growth medium was replaced with a mixture of 50% conditioned, and 50% fresh growth medium. The transfection process was as follows: 4 µg cDNA was mixed in a 50 µl total with Opti-MEM (Thermo Fisher), 2 µl Lipofectamine 2000 (Thermo Fisher) was mixed in a 50 µl total volume of Opti-MEM in separate tubes by pipetting; mixing was done by gentle pipetting. DNA and transfection reagent mixes were then combined and incubated for 5 min at room temperature before being added dropwise to cultures. Hippocampal neurons were cultured for a further 7 d after transfection before fixation and immunostaining.

Immunocytochemistry. Cells were plated onto either 20 mm square coverslips, or glass-bottomed dishes (MatTek Corporation) which were coated with poly-L-lysine prior to transfection, and cultured in a 5% CO_2 incubator at 37 °C. After 36–48 h expression, cells were fixed with ice cold 4% paraformaldehyde (PFA), 4% sucrose in PBS, pH 7.4 at room temperature for 5 min. Where antigen retrieval was used, fixed samples were incubated in pH 6 citrate buffer at 98˚C for 10 min[10]. For labelling the HA epitope on the cell-surface in non-permeabilised conditions, cells were incubated with primary Ab with 2% BSA and 10% goat serum in PBS at room temperature for 1 h for cell lines or overnight at 4 °C for neurons (Fig. 3). Using the same protocol, no detectable permeabilization by PFA fixation in hippocampal neurons was observed in a previous study[51]. When permeabilization was required, cells were incubated with 0.2% Triton X-100 in PBS for 5 min[10]. The secondary Ab was added with 2.5% BSA and 10% goat serum in PBS and incubated for 1 h at room temperature. Cell nuclei were stained with 0.5 µM 4′,6′-diamidino-2-phenylindole (DAPI) in PBS for 10 min. The coverslips were mounted onto glass slides using Vectashield mounting medium (Vector Laboratories).

In experiments probing for both cell-surface and intracellular HA epitopes (Fig. 1), cells were fixed and blocked as described above, then immunostained for 1 h with rat anti-HA Ab (1:500), followed by 1 h incubation with biotin-labelled anti-rat IgG (1:1000). Following this, cells were permeabilised with 0.2% Triton-X100 for 5 min and re-probed with rat anti-HA Ab for 1 h. Cells were then incubated with anti-rat-AF594 Ab (1:500) and streptavidin-AF633 (1:500), to visualise intracellular and extracellular HA epitopes, respectively. In experiments probing for cell surface BBS tag in $Ca_V2.2$ (Fig. 2, Fig. S1), cells were live-labelled with BTX-AF488 (10 µg/ml, Invitrogen) for 30 min at 17 °C. Cells were then washed, fixed, permeabilised and immunostained, using a rabbit Ab against the II-III loop to detect total $Ca_V2.2$, followed by secondary anti-rabbit-AF594 Ab.

Net forward trafficking assay. Transfected cells were plated onto 22 × 22 mm glass coverslips coated with poly-L-lysine, and cultured in a 5% CO_2 incubator at 37 °C. N2a cells were used for $Ca_V2.2$-HA experiments and tsA-201 cells for $\alpha_2\delta$-1 experiments, where higher expression levels were required to observe live labelling. After 40 h expression, cells were washed twice with Krebs–Ringer-HEPES (KRH) buffer and incubated with 10 µg/ml unlabelled BTX (Life technologies) for 30 min at 17 °C. The unbound BTX was washed off with KRH, and the cells were then incubated with BTX-AF488 (10 µg/ml) in KRH at 37 °C. To terminate the reaction, cells were washed twice with cold KRH and then fixed with 4% PFA, 4% sucrose in PBS at specified times for the kinetic assay. After fixation, cells were permeabilised and intracellular expression markers and/or nuclei were labelled as described above. The coverslips were then mounted onto glass slides using Vectashield mounting medium.

Confocal microscopy and analysis. All images were acquired using an LSM 780 scanning confocal microscope (Zeiss), equipped with a Plan-Apochromat 63x/1.4 or 40x/1.3 DICII oil immersion objective lens, in 16-bit mode. For experiments in which both AF594 and AF633 were used, sequential scanning was performed with 633 nm and 594 nm laser lines, with emission filters 638–747 nm or 597–695 nm, with beam splitters (MBS) 488/543/633 and MBS 458/514/594, respectively. For each experiment, the laser power, gain and acquisition settings were kept constant between images that were used for quantification, although laser power and gain settings were adjusted between experiments depending on expression and staining level of the samples. Where possible, the region of interest was determined by identifying cells with expression of a transfection marker or intracellular staining of the protein of interest (e.g. GFP, HA), without selecting for the cell-surface immunostaining, to avoid bias. In experiments where an appropriate intracellular expression marker was absent,

nuclear staining with DAPI was used to identify viable cells (having an intact nucleus); cell-surface measurements were made for all viable cells per field of view. In addition, a 2 × 2 or 3 × 3 tile scan was performed to further remove the bias in selecting cells with high expression. For cell-surface expression analysis, images were taken usually with 1 µm optical section. Confocal images were imported and analysed in ImageJ (National Institutes of Health). The plasma membrane fluorescence was quantified using the freehand brush tool with a selection width of 0.66 µm and tracing the membrane region manually. If any cells show signs of intracellular staining for the extracellular epitope, because of damage-induced permeabilization, they are excluded from analysis. Total or intracellular fluorescence was quantified using the freehand selection tool, omitting the signal intensity from the nuclei. The background fluorescence in each channel was measured and subtracted from mean cell-surface or intracellular fluorescence measurements in image analysis.

For analysis of neurite expression in hippocampal neurons, an average of 10–15 cells were selected per condition for an individual experiment. Neurons were selected based on expression of free mCherry as a transfection marker. Between 2 and 5 neurites (with the appearance of dendrites) were measured per mCherry-positive cell to reduce over-representation of highly branched neurons. The freehand brush tool was used to manually trace neurites of lengths between 25 and 60 µm, and width of 2 µm, beginning at a distance of 100 µm from the cell soma. Neurites were selected and traced using mCherry to avoid bias, measurements were then taken in channels for expression of HA and/or GFP tags on expressed $Ca_V2.2$ constructs. Background fluorescence measurements were taken for each condition and subtracted from mean fluorescence values during image analysis. Mean neurite signal intensity for each channel was calculated for neurons of a given condition and normalized to the stated controls. Normalized data were then pooled between experiments with a minimum of three separate experiments.

In cell-surface expression and forward trafficking experiments, where relevant, all cells chosen for analysis contained intracellular $Ca_V2.2$ expression. For the forward trafficking assays, the membrane fluorescent intensities were fitted to the single exponential association. All experiments were repeated n = 3–5 times, and approximately 30–50 cells were analysed for each experiment. All data are presented as pooled cells, except for the trafficking initial rates, which are averages of separate experiments.

Electrophysiology. tsA-201 cells were transfected with cDNA mix containing $Ca_V2.2$, $\alpha_2\delta$-1, β1b, and CD8 at a ratio of 3:2:2:0.8 using a Fugene transfection protocol. After 40 h expression, cells were replated in cell culture medium at 1 in 3 or 1 in 5 dilution depending on their confluency. Transfected cells were identified by CD8 expression, detected with CD8 Dynabeads (Life Technologies). Whole-cell currents were recorded in voltage-clamp mode in the following solutions; intracellular solution (mM): 140 Cs-aspartate, 5 EGTA, 2 $MgCl_2$, 0.1 $CaCl_2$, 2 K_2ATP, 20 HEPES, pH 7.2, 310 mOsm; extracellular solution (mM): 1 $BaCl_2$, 3 KCl, 1 $NaHCO_3$, 1 $MgCl_2$, 10 HEPES, 4 D-glucose, 160 tetraethylammonium bromide, pH 7.4, 320 mOsm. The borosilicate glass electrode resistance was between 1.5 and 4 MΩ. Cell capacitance and series resistance were compensated to 60–70%. Whole-cell currents were recorded on Axopatch-200B amplifier using pClamp 9 or 10 (Molecular Devices). The cells were held at − 90 mV, and 50 ms pulses were applied in + 10 mV steps between − 50 mV and + 50 mV. To correct for the leak current, P/8 leak subtraction protocol was applied. Recordings were made at 20 kHz sampling frequency and filtered at 5 kHz (lowpass 4-pole Bessel filter) in the amplifier. The digital low-pass 8-pole Bessel filter with 1 kHz 3 dB cut-off was applied in Clampfit 10.7 (Molecular Devices) before the current amplitudes were determined. Average peak currents were taken between 8 and 13 ms after the test potentials were applied and normalized to the cell capacitance to obtain current density. *IV* relationships were fit by a modified Boltzmann equation as follows: $I = G_{max}*(V-V_{rev})/(1+exp(-(V-V_{50,\,act})/k))$, where I is the current density (in pA/pF), G_{max} is the maximum conductance (in nS/pF), V_{rev} is the apparent reversal potential (mV), $V_{50,\,act}$ is the midpoint voltage for current activation (mV), and k is the slope factor.

Statistical analysis. The number of samples (n) in most of the experiments in this study is the total number of individual cells analysed, which are pooled from a minimum of three separate experiments unless stated otherwise. Data from individual experiments were normalized to their control conditions prior to being pooled to account for inter-experimental variance. Mean values and standard error of mean (SEM) were calculated for normalized, pooled data. The only exception is for the experiments determining the rates of $Ca_V2.2$ trafficking, where the mean and SEM values were determined from the mean of repeated experiments. Statistical analysis was performed using Student's t test or one-way ANOVA with appropriate post-hoc test as stated, in GraphPad Prism 7.

Ethical approval. The use of neonatal mice for primary hippocampal cultures was carried out according to methods covered by UK Home Office Schedule I procedures. Ethical approval for Schedule I licence 1285 was obtained from the local UCL Animal Welfare Ethical Review Body (AWERB) and followed ARRIVE guidelines and regulations.

Received: 1 March 2021; Accepted: 16 April 2021
Published online: 13 May 2021

References

1. Dolphin, A. C. Voltage-gated calcium channels: their discovery, function and importance as drug targets. *Brain Neurosci. Adv.* **2**, 239821281879480 (2018).

2. De Jongh, K. S., Merrick, D. K. & Catterall, W. A. Subunits of purified calcium channels: a 212-kDa form of a_1 and partial amino acid sequence of a phosphorylation site of an independent b subunit. *Proc. Natl. Acad. Sci. U.S.A.* **86**, 8585–8589 (1989).
3. Jay, S. D. *et al.* Structural characterization of the dihydropyridine-sensitive calcium channel a_2-subunit and the associated d peptides. *J. Biol. Chem.* **266**, 3287–3293 (1991).
4. Davies, A. *et al.* The a2d subunits of voltage-gated calcium channels form GPI-anchored proteins, a post-translational modification essential for function. *Proc. Natl. Acad. Sci. USA* **107**, 1654–1659 (2010).
5. Dolphin, A. C. Voltage-gated calcium channels and their auxiliary subunits: physiology and pathophysiology and pharmacology. *J Physiol* **594**, 5369–5390 (2016).
6. Felix, R., Gurnett, C. A., De Waard, M. & Campbell, K. P. Dissection of functional domains of the voltage-dependent Ca2+ channel alpha2delta subunit. *J. Neurosci.* **17**, 6884–6891 (1997).
7. Gurnett, C. A., De Waard, M. & Campbell, K. P. Dual function of the voltage-dependent Ca^{2+} channel a_2d subunit in current stimulation and subunit interaction. *Neuron* **16**, 431–440 (1996).
8. Wakamori, M., Mikala, G. & Mori, Y. Auxiliary subunits operate as a molecular switch in determining gating behaviour of the unitary N-type Ca2+ channel current in Xenopus oocytes. *J. Physiol.-Lond.* **517**, 659–672 (1999).
9. Barclay, J. *et al.* Ducky mouse phenotype of epilepsy and ataxia is associated with mutations in the *Cacna2d2* gene and decreased calcium channel current in cerebellar Purkinje cells. *J. Neurosci.* **21**, 6095–6104 (2001).
10. Cassidy, J. S., Ferron, L., Kadurin, I., Pratt, W. S. & Dolphin, A. C. Functional exofacially tagged N-type calcium channels elucidate the interaction with auxiliary alpha2delta-1 subunits. *Proc. Natl. Acad. Sci. USA* **111**, 8979–8984 (2014).
11. Hendrich, J. *et al.* Pharmacological disruption of calcium channel trafficking by the a2d ligand gabapentin. *Proc. Natl. Acad. Sci. USA* **105**, 3628–3633 (2008).
12. Davies, A. *et al.* The calcium channel a2d–2 subunit partitions with CaV2.1 in lipid rafts in cerebellum: implications for localization and function. *J. Neurosci.* **26**, 8748–8757 (2006).
13. Canti, C. *et al.* The metal-ion-dependent adhesion site in the Von Willebrand factor-A domain of alpha2delta subunits is key to trafficking voltage-gated Ca2+ channels. *Proc. Natl. Acad. Sci. USA* **102**, 11230–11235 (2005).
14. Kadurin, I. *et al.* Proteolytic maturation of α2δ represents a checkpoint for activation and neuronal trafficking of latent calcium channels. *Elife* **5**, e1143 (2016).
15. Ferron, L., Kadurin, I. & Dolphin, A. C. Proteolytic maturation of alpha2delta controls the probability of synaptic vesicular release. *Elife* **7**, e37507 (2018).
16. Tran-Van-Minh, A. & Dolphin, A. C. The alpha2delta ligand gabapentin inhibits the Rab11-dependent recycling of the calcium channel subunit alpha2delta-2. *J. Neurosci.* **30**, 12856–12867 (2010).
17. Li, G. & Marlin, M. C. Rab family of GTPases. *Methods Mol. Biol.* **1298**, 1–15 (2015).
18. Ren, M. *et al.* Hydrolysis of GTP on rab11 is required for the direct delivery of transferrin from the pericentriolar recycling compartment to the cell surface but not from sorting endosomes. *Proc. Natl. Acad. Sci. U S A* **95**, 6187–6192 (1998).
19. Ullrich, O., Reinsch, S., Urbe, S., Zerial, M. & Parton, R. G. Rab11 regulates recycling through the pericentriolar recycling endosome. *J. Cell Biol.* **135**, 913–924 (1996).
20. Eisfeld, A. J., Kawakami, E., Watanabe, T., Neumann, G. & Kawaoka, Y. RAB11A is essential for transport of the influenza virus genome to the plasma membrane. *J. Virol.* **85**, 6117–6126 (2011).
21. Field, M. J. *et al.* Identification of the a2d–1 subunit of voltage-dependent calcium channels as a novel molecular target for pain mediating the analgesic actions of pregabalin. *Proc. Natl. Acad. Sci. USA* **103**, 17537–17542 (2006).
22. Gee, N. S. *et al.* The novel anticonvulsant drug, gabapentin (Neurontin), binds to the a_2d subunit of a calcium channel. *J. Biol. Chem.* **271**, 5768–5776 (1996).
23. Lotarski, S. M. *et al.* Anxiolytic-like activity of pregabalin in the Vogel conflict test in alpha2delta-1 (R217A) and alpha2delta-2 (R279A) mouse mutants. *J. Pharmacol. Exp. Ther* **338**, 615–621 (2011).
24. Lotarski, S. *et al.* Anticonvulsant activity of pregabalin in the maximal electroshock-induced seizure assay in alphadelta (R217A) and alphadelta (R279A) mouse mutants. *Epilepsy Res.* **108**, 833–842 (2014).
25. Wang, M. H., Offord, J., Oxender, D. L. & Su, T. Z. Structural requirement of the calcium-channel subunit a_2d for gabapentin binding. *Biochem. J.* **342**, 313–320 (1999).
26. Macabuag, N. & Dolphin, A. C. Alternative splicing in CaV2.2 regulates neuronal trafficking via adaptor protein complex-1 adaptor protein binding motifs. *J. Neurosci.* **35**, 14636–14652 (2015).
27. Dahimene, S. *et al.* The a_2d-like protein cachd1 increases N-type calcium currents and cell surface expression and competes with a_2d–1. *Cell Rep.* **25**, 1610–1621 (2018).
28. Geisler, S. *et al.* Presynaptic alpha2delta-2 calcium channel subunits regulate postsynaptic GABAA receptor abundance and axonal wiring. *J. Neurosci.* **39**, 2581–2605 (2019).
29. Bikbaev, A. *et al.* Auxiliary alpha2delta1 and alpha2delta3 subunits of calcium channels drive excitatory and inhibitory neuronal network development. *J. Neurosci.* **40**, 4824–4841 (2020).
30. Brown, J. P., Dissanayake, V. U., Briggs, A. R., Milic, M. R. & Gee, N. S. Isolation of the [3H]gabapentin-binding protein/alpha 2 delta Ca2+ channel subunit from porcine brain: development of a radioligand binding assay for alpha 2 delta subunits using [3H] leucine. *Anal. Biochem* **255**, 236–243 (1998).
31. Dolphin, A. C. Voltage-gated calcium channel alpha 2delta subunits: an assessment of proposed novel roles. *F1000Res* **7**, 1830 (2018).
32. Kadurin, I., Rothwell, S. W., Lana, B., Nieto-Rostro, M. & Dolphin, A. C. LRP1 influences trafficking of N-type calcium channels via interaction with the auxiliary alpha2delta-1 subunit. *Sci. Rep.* **7**, 43802 (2017).
33. Lillis, A. P., Van Duyn, L. B., Murphy-Ullrich, J. E. & Strickland, D. K. LDL receptor-related protein 1: unique tissue-specific functions revealed by selective gene knockout studies. *Physiol. Rev.* **88**, 887–918 (2008).
34. Brockhaus, J. *et al.* alpha-neurexins together with alpha2delta-1 auxiliary subunits regulate Ca(2+) influx through Cav2.1 channels. *J. Neurosci.* **38**, 8277–8294 (2018).
35. Tong, X.-J. *et al.* Retrograde synaptic inhibition is mediated by α-neurexin binding to the α2δ subunits of N-type calcium channels. *Neuron* **95**, 1–15 (2017).
36. Eroglu, C. *et al.* Gabapentin receptor alpha2delta-1 Is a neuronal thrombospondin receptor responsible for excitatory CNS synaptogenesis. *Cell* **139**, 380–392 (2009).
37. Lana, B. *et al.* Thrombospondin-4 reduces binding affinity of [3H]-gabapentin to calcium-channel α2δ-1-subunit but does not interact with α2δ-1 on the cell-surface when co-expressed. *Sci. Rep.* **6**, 24531 (2016).
38. El-Awaad, E. *et al.* Direct, gabapentin-insensitive interaction of a soluble form of the calcium channel subunit alpha2delta-1 with thrombospondin-4. *Sci. Rep.* **9**, 16272 (2019).
39. van Bergeijk, P., Adrian, M., Hoogenraad, C. C. & Kapitein, L. C. Optogenetic control of organelle transport and positioning. *Nature* **518**, 111–114 (2015).
40. Homma, Y. & Fukuda, M. Rabin8 regulates neurite outgrowth in both GEF activity-dependent and -independent manners. *Mol. Biol. Cell* **27**, 2107–2118 (2016).
41. Goldenring, J. R. Recycling endosomes. *Curr. Opin. Cell Biol* **35**, 117–122 (2015).
42. Kurshan, P. T., Oztan, A. & Schwarz, T. L. Presynaptic alpha(2)delta-3 is required for synaptic morphogenesis independent of its Ca(2+)-channel functions. *Nat. Neurosci* **12**, 1415–1423 (2009).

43. Pragnell, M., Sakamoto, J., Jay, S. D. & Campbell, K. P. Cloning and tissue-specific expression of the brain calcium channel b-subunit. *FEBS Lett.* **291**, 253–258 (1991).
44. Kim, H.-L., Kim, H., Lee, P., King, R. G. & Chin, H. Rat brain expresses an alternatively spliced form of the dihydropyridine-sensitive L-type calcium channel a2 subunit. *Proc. Natl. Acad. Sci. U.S.A.* **89**, 3251–3255 (1992).
45. Kadurin, I. *et al.* Calcium currents are enhanced by alpha2delta-1 lacking its membrane anchor. *J. Biol. Chem* **1287**, 33554–33566 (2012).
46. Shaner, N. C. *et al.* Improved monomeric red, orange and yellow fluorescent proteins derived from Discosoma sp. red fluorescent protein. *Nat. Biotechnol.* **22**, 1567–1572 (2004).
47. Rougier, J. S. *et al.* Molecular determinants of voltage-gated sodium channel regulation by the Nedd4/Nedd4-like proteins. *Am. J. Physiol. Cell Physiol.* **288**, C692-701 (2005).
48. Dupre, D. J. *et al.* Seven transmembrane receptor core signaling complexes are assembled prior to plasma membrane trafficking. *J. Biol. Chem.* **281**, 34561–34573 (2006).
49. Raghib, A. *et al.* Dominant-negative synthesis suppression of voltage-gated calcium channel Cav2.2 induced by truncated constructs. *J. Neurosci.* **21**, 8495–8504 (2001).
50. Niwa, H., Yamamura, K. & Miyazaki, J. Efficient selection for high-expression transfectants with a novel eukaryotic vector. *Gene* **108**, 193–199 (1991).
51. Meyer, J. O. *et al.* Disruption of the key Ca^{2+} binding site in the selectivity filter of neuronal voltage-gated calcium channels inhibits channel trafficking. *Cell Rep.* **29**, 22–33 (2019).

Acknowledgements

The authors thank Wendy S Pratt and Kanchan Chaggar for technical support, and Dr. Laurent Ferron and Kjara Pilch for hippocampal cultures. We thank Drs. Karen Page and Manuela Nieto-Rostro for commenting on the manuscript.

Author contributions

J.O.M. performed all experimental work, and analysed data. A.C.D. analysed data. J.O.M. and A.C.D. conceived the study, co-wrote the manuscript and prepared the Figures.

Funding

This research was funded, in part, by the Wellcome Investigator award to ACD (098360/Z/12/Z)]. For the purpose of Open Access, the corresponding author has applied a CC BY public copyright licence to any Author Accepted Manuscript version arising from this submission. JOM was supported in part by the UCL Grand Challenges PhD program.

Competing interests

The authors declare no competing interests.

Additional information

Supplementary information The online version contains supplementary material available at https://doi.org/10.1038/s41598-021-89820-1.

Correspondence and requests for materials should be addressed to A.C.D.

Reprints and permissions information is available at www.nature.com/reprints.

Publisher's note Springer Nature remains neutral with regard to jurisdictional claims in published maps and institutional affiliations.